7/16/1999

Azimuth Track Level Compensation to Reduce Blind Pointing Errors of the Deep Space Network Antennas

Wodek Gawronski[1], Farrokh Baher[1], and Ofelia Quintero[2]

Jet Propulsion Laboratory
California Institute of Technology
[1]Communications Ground System Section
[2]Space Instruments Implementation Section
Pasadena, CA 91109
Tel.: (818) 354-1783
Fax: (818) 393-0207
E-mail: wodek.k.gawronski@jpl.nasa.gov

1. Abstract

The beam wave-guide antennas of the NASA Deep Space Network are "wheel and track" antennas. The latter term refers to a set of wheels at the base of the structure, which roll on a circular steel track supported by a concrete foundation ring. The track is assumed flat, however its level varies due to manufacturing imperfections, structural loads, non-uniformity of the soil, and temperature variations. It is specified that the deviations of the level of azimuth track shall not exceed ±0.02 in (or ±0.5 mm). During tracking these rather small deviations cause deformations of antenna structure, and result in pointing errors of ±2 mdeg, which exceeds the required accuracy for Ka-band tracking. However, the structural deformations caused by the azimuth track unevenness are repeatable, therefore a look-up table can be created to improve the blind-pointing accuracy. This paper presents the process of a creation of the look-up table, describes

the instrumentation necessary for the determining the pointing errors, and describes the processing of inclinometer data. It derives algorithms for the pointing error estimation and for the azimuth axis tilt using the inclinometer data, and compares the error corrections based on the created look-up table and actual measurements of pointing errors using conscan technique. This comparison shows a satisfactory convergence that justifies the implementation of the approach in the forthcoming NASA missions.

2. Introduction

The NASA Deep Space Network (DSN) antennas serve as a communication tools for the space exploration. An example of the NASA/JPL beam-wave guide antenna with 34-meter dish is shown in Fig.1. The antenna can rotate with respect to the azimuth (vertical) and elevation (horizontal) axes. Rotation in azimuth is accomplished by moving the entire structure on a circular azimuth track. The track, however, is manufactured with level precision of ±0.02 in (or ±0.5 mm). The uneven azimuth track level causes antenna tilts and flexible deformations, which deteriorate its pointing accuracy. Preliminary analysis indicated that this level of deviations could cause pointing errors exceeding Ka-band tracking requirement of 1.5 mdeg. However, the pointing errors caused by the track irregularities are repeatable therefore they can be calibrated. By developing a look-up table one provides pointing corrections as a function of the antenna azimuth position. The look-up table is generated by using inclinometers to measure tilts of the alidade structure at selected points. The effectiveness of this procedure is ultimately checked by the measurement of the antenna pointing error during tracking.

The task of the blind pointing error correction due to track level unevenness consists of the following steps, described subsequently in this paper:

- carrying out finite element analysis of the alidade structure to select inclinometer locations,
- developing algorithms to determine (a) the pointing errors, (b) azimuth axis tilt, and (c) azimuth track profile from inclinometer data,

- choosing optimal azimuth rate for data collection, collecting data, and verifying the pointing model through the antenna wheel shimming,
- processing data, checking repeatability and smoothing the data,
- creating the look-up table,
- verifying the blind pointing error correction table using conscan.

3. Hardware and Software Description

Hardware components of the track level compensation system consist of eight inclinometers, an interface assembly, an industrial PC computer and several single based computer boards (A/D and digital I/O data acquisition cards). The communication between the different components of the system is through a parallel port.

Eight surface mount inclinometers, Model 711-2 of Applied Geomechanics, are mounted at the antenna. These low power, dual-axis, analog output inclinometers contain temperature sensors. The interface box is used to process the inclinometer and antenna azimuth encoder data to the format acceptable by a PC computer. The data are collected via A/D and digital I/O boards installed in the computer. These based computer boards allow for the recording of the inclinometers and azimuth encoder data.

The software components of the system include Windows NT (real time operations), Labview (an instrumentation and graphical programming), and Matlab (an analysis tool). The data was monitored and collected using the Labview and were post-processed and analyzed by Matlab.

4. Inclinometer Data

Eight inclinometers were installed on the alidade structure, and their locations are marked in Fig.2. Each inclinometer measures tilts of its x- and y-axes. The locations of the inclinometers were selected using the finite element analysis of the alidade structure. The inclinometers are located such that their tilts can be used to estimate the alidade elevation and cross-elevation rotations next to the antenna focal point. Inclinometers No.1 and 2 are located at the top of the alidade. Inclinometer No.2 is located next to the elevation encoder. Thus the y-axis tilt of this inclinometer reflects the elevation pointing

error. Inclinometers No 7 and 8 are located in the middle of the crossbeam of the left and right sides of the alidade, respectively. Their x-axis tilts combined with the x-axis tilts of the inclinometers No.1 and 2, give the cross-elevation pointing error, as it will be shown later in this paper. Inclinometers No 3, 4, 5,and 6 are used for checking accuracy of the cross-elevation error model, and are also used for the determination of the azimuth track profile. In the following the x- and y-axis tilts of the ith inclinometer are denoted α_{ix} and α_{iy}, respectively.

The inclinometer data were collected during the antenna azimuth rotation with constant rate of 50 mdeg/s, at the sampling frequency of 2 Hz. The rate of 50 mdeg/s was selected after testing different rates, and measuring the noise level, temperature gradient impact (by checking the repeatability of the data). Low rate data have lower noise level but larger repeatability error than high rate data: in the larger time span of the data collection larger thermal deformations were observed. The tests were performed during nighttime to minimize distortions of the antenna structure due to the thermal gradient. We collected 6 sets of data for full (0-360 deg) azimuth rotations, four for the clockwise rotations, and two for the counterclockwise rotations. The data show satisfactory repeatability in the clockwise direction, see Fig.3 for the data collected at inclinometer No1. There are some drifts due to factors, such as temperature variations - there was about 3 hours shift between each data collection at night.

The alidade deformation due to temperature drift was recorded while antenna was stowed. A sample of the inclinometer data is shown in Fig.4. From this figure one can see that within the time span of 3 hours at night the temperature change causes the inclinometer drift about 0.5 mdeg. During the day the time span of 3 hours may cause as much as 4-mdeg elevation tilt.

Do the errors caused by the azimuth track unevenness depend on the antenna elevation position? This question was answered by collecting data for the antenna elevation angles of 15, 45, 60, and 89 deg. All inclinometer readings were the same (within the instrument accuracy), showing that the azimuth track profile pointing errors do not depend on the antenna elevation position.

The data were smoothed using zero-phase lowpass-filter, see for example Ref.[1]. This filter smoothes the data without shifting them. The longer averaging, the smoother is the curve. It was determined that the length of 50 smoothes small "bumps" that are non-desirable in the look-up table.

5. Determining Pointing Errors

The *y*-tilt of the second inclinometer is a rotation with respect to the antenna *x*-axis, denoted δ_x. It is a measure of the antenna elevation error Δ_{el}

$$\Delta_{el} = \delta_x = \alpha_{2y} \tag{1}$$

see Fig.5.

The cross-elevation error (Δ_{xel}) depends on the antenna elevation position (θ_{el}). It depends also on the rotation (δ_y) of the top of the alidade with respect to the *y*-axis (tilt of the elevation axis) and the alidade twist δ_z (the rotation of the top of the alidade with respect to the *z*-axis):

$$\Delta_{xel} = \delta_z \cos(\theta_{el}) - \delta_y \sin(\theta_{el}) \tag{2}$$

see Fig.6. The orientation of axes *x, y,* and *z* with respect to antenna dish is explained in Fig.7.

The tilt of the elevation axis is an average of the *x*-tilts of the inclinometers 1 and 2, that is,

$$\delta_y = 0.5(\alpha_{1x} + \alpha_{2x}) \tag{3}$$

while the alidade twist is not directly measured by inclinometers. It is determined from *x*-tilts of the inclinometer No7 and No8, by assuming that these tilts are satisfactory measures of the horizontal displacements of the top of the antenna (for justification see

Appendix A). Based on this assumption the following estimate of the antenna twist was obtained, see Appendix A

$$\delta_z = \frac{h(\alpha_{7x} - \alpha_{8x})}{l} \tag{4}$$

where h is the alidade height, and l is the distance between the inclinometers 1 and 2, see Fig.A1 in the Appendix A. Since $h/l = 1.245$, we found that

$$\delta_z = 1.245(\alpha_{7x} - \alpha_{8x}) \tag{5}$$

Combining equations (2), (3), and (5), the cross-elevation pointing error is determined from the x-tilts of the inclinometers 1,2,7,8 as follows

$$\Delta_{xel} = 1.245(\alpha_{7x} - \alpha_{8x})\cos(\theta_{el}) - 0.5(\alpha_{1x} + \alpha_{2x})\sin(\theta_{el}) \tag{6}$$

The azimuth error is a function of the cross-elevation error

$$\Delta_{az} = \frac{\Delta_{xel}}{\cos(\theta_{el})} \tag{7}$$

therefore

$$\Delta_{az} = \delta_z - \delta_y \tan(\theta_{el}) \tag{8}$$

or

$$\Delta_{az} = 1.245(\alpha_{7x} - \alpha_{8x}) - 0.5(\alpha_{1x} + \alpha_{2x})\tan(\theta_{el}) \tag{9}$$

The accuracy of the assumption of using side inclinometers as estimators of the horizontal displacements of the alidade top is checked using the inclinometer field data, see Fig.8. In these data the plots of the top, middle, and bottom tilts of the alidade sides were determined. The first two were directly measured by inclinometers 1, 2, 7, 8, the bottom tilt was derived from x-tilts of inclinometers 3,4,5,6. The antenna shimming, as described in the following section, relates the x-tilts of inclinometers 3,4,5,6 to the wheel (or lower beam end) displacement. The difference between the beam end displacements divided by the beam length gave the lower beam tilt. These tilts show flexible deformations on top of the rigid body motion (for pure rigid body motion these three angles would be identical). The middle beam angle was chosen as an estimator of the top horizontal displacement. Its accuracy can be verified through the averaging of the rotations of the top and the bottom locations. Figure 9 shows satisfactory convergence between the middle beam rotation and the average rotation of the bottom and the top locations.

The δ_x, δ_y, and δ_z alidade rotations were smoothed for azimuth angles varied from 0 to 360 deg, for 0.1 deg azimuth angle sample size. Their plots are shown in Fig.10. These three plots for the error correction data used in Eqs.(1) and (2).

6. Determining Track Profile

The wheel shimming and tilt measurements were conducted to show the relationship between the inclinometer tilt and the azimuth track unevenness. For the inclinometers No.3, 4, 5, 6 it was 14.8 mdeg x-tilt for the 0.1 inch of wheel lift. Based on this scaling and the continuous records of the lower inclinometer x-tilt measurements during the antenna constant rate slewing the azimuth track profile was determined, and is shown in Fig.11. It is seen from this plot that the maximum, peak-to-peak, track profile variation is 0.048 inch, slightly higher than the specification (0.040 inch), see JPL Document TP 515904 .

7. Determining Azimuth Axis Tilt

Using the inclinometer data one can determine the azimuth axis tilt. It is represented as a sinusoidal component in the inclinometer measurements. Its amplitude a and phase φ need to be determined. Let $\alpha_{1x}(i)$ and $\alpha_{1y}(i)$ be the ith sample of the x- and y-tilts of the inclinometer 1, and *e(i)* be the ith sample of the azimuth encoder. The inclinometer harmonics caused by the azimuth axis tilt are described as

$$\alpha_{1x}(i) = a\cos(e(i)+\varphi), \quad \text{and} \quad \alpha_{1y}(i) = a\sin(e(i)+\varphi) \tag{10}$$

The amplitude and phase of the tilt are determined as follows (for the derivation see Appendix B)

$$a = \sqrt{A_{11}^2 + A_{21}^2}, \quad \text{and} \quad \varphi = \tan^{-1}\left(\frac{A_{21}}{A_{11}}\right) \tag{11}$$

where $A = \begin{Bmatrix} A_{11} \\ A_{21} \end{Bmatrix}$ is obtained from the following equation

$$A = (P^T P)^{-1} P^T \alpha_1 \tag{12}$$

In this equation

$$\alpha_1 = \begin{Bmatrix} \alpha_{1x} \\ \alpha_{1y} \end{Bmatrix}, \text{ where } \alpha_{1x} = \begin{Bmatrix} \alpha_{1x}(1) \\ \alpha_{1x}(2) \\ \vdots \\ \alpha_{1x}(n) \end{Bmatrix}, \quad \alpha_{1y} = \begin{Bmatrix} \alpha_{1y}(1) \\ \alpha_{1y}(2) \\ \vdots \\ \alpha_{1y}(n) \end{Bmatrix} \tag{13a}$$

and

$$P=\begin{bmatrix} c & -s \\ s & c \end{bmatrix}, \text{ where } c=\begin{Bmatrix} c_1 \\ c_2 \\ \vdots \\ c_n \end{Bmatrix}, \quad s=\begin{Bmatrix} s_1 \\ s_2 \\ \vdots \\ s_n \end{Bmatrix} \tag{13b}$$

Based on several sets of data we obtained from (11) the following amplitude and phase of the azimuth axis tilt

$a = 1.6$ mdeg, and φ = -64 deg

The plots of the inclinometer tilts with the best-fit sinusoid of the azimuth axis tilt are shown in Figs.12a and 13a. The sinusoid was subtracted from the inclinometer data, and the residuals are shown in Figs.12b and 13b. They show that even for the perfectly vertical azimuth axis the pointing error due to azimuth track unevenness is 4-6 mdeg, peak-to-peak, and it is repeatable.

8. Verification of the Look-Up Table Using Conscan Measurements

On DOY-349 of 1997 conscan pointing errors have been measured, while tracking continuously a single point source (0927+390) for 8 hours, from 10 p.m. to 6 a.m. local time for azimuth range 305 – 330 and 0 – 50 deg. The conscan derived pointing errors are shown as dots in Figs.14a,b,c,d while the inclinometer derived pointing errors are shown as a solid line. The results show a significant correlation between the conscan and inclinometer derived errors. Each data set shows agreement at the sub-milidegree level.

9. Conclusions

The alidade three-axis rotation table as a function of the antenna azimuth position has been obtained from the measured inclinometer tilts. From this table the antenna pointing errors are derived. These errors were compared with the conscan-derived errors

showing good coincidence, and the potential to reduce the blind pointing by 2-3 mdeg. The procedure was designed as a look-up table to compensate for the azimuth track level unevenness. It shows a potential as an on-line measuring device to compensate for all errors caused by the alidade tilts (this includes azimuth track unevenness, azimuth axis tilt and thermal deformations).

10. Acknowledgments

The authors would like to thank Chris Yung for the recognizing the problem, initializing it, and discussions of technical problems; John Cucchissi and Mark Gatti - for technical discussions and leadership; Ian Pain of James Clerk Maxwell Telescope of Mauna Kea, Hawaii for the advice in the initialization of this research; Paul Richter and David Rochblatt - for conscan data collection and discussions that allowed improving the paper; Tim Sink for helping in the antenna measurements; and Hal Ahlstrom - for discussions that resolved several technical problems.

11. References

1. S.D. Stearns, and D.R. Hush, *Digital Signal Analysis,* Prentice Hall, Englewood Cliffs, 1990.

Appendix A.

Derivation of the Cross-Elevation Pointing Error from the Inclinometer Data

The cross-elevation error (Δ_{xel}) depends on the antenna elevation position (θ_{el}). It depends also on the rotation (δ_y) of the top of the alidade with respect to the *y*-axis (tilt of the elevation axis), and the alidade twist δ_z (the rotation of the top of the alidade with respect to the *z* axis), i.e.,

$$\Delta_{xel} = \delta_z \cos(\theta_{el}) - \delta_y \sin(\theta_{el}) \tag{A1}$$

see Fig.6.

The tilt of the elevation axis is an average of the *x*-tilts of the inclinometers 1 and 2, that is,

$$\delta_y = 0.5(\alpha_{1x} + \alpha_{2x}) \tag{A2}$$

while the alidade twist is not directly measured by inclinometers. It is determined as follows. From Fig.A1

$$\delta_z = \frac{\Delta x_2 - \Delta x_1}{l} \tag{A3}$$

where Δx_1 and Δx_2 are horizontal displacements of the locations of inclinometers 1 and 2, and l=488 inches is the distance between the two inclinometers. The displacements Δx_1 and Δx_2 are determined from the tilts of inclinometers 8 and 7, respectively, by assuming that the horizontal displacement of the alidade side due to azimuth track unevenness is caused predominantly by the rigid-body motion of each side of the alidade, as shown in Fig.A2. This assumption was checked with the finite element model of the alidade, see Fig.A3. Using finite element model we determined displacements Δx_1 and Δx_2 assuming the rigid-body rotation of the bottom beam and

compared it to the actual displacements Δx_1 and Δx_2 that included flexible deformations. The difference was 18% with respect to true rotations. If the displacement were determined using the rigid body assumption and the rotation of the middle beam the error in Δx_1 and Δx_2 displacements is less than 7%. Thus, the middle beam rotation was selected as a rigid body rotation estimator. This angle is measured as the x-tilt of the inclinometers 7 and 8 (denoted as α_{7x} and α_{8x}, respectively). The top displacements Δx_1 and Δx_2 of the alidade are obtained from the rigid-body angles as follows, based on the alidade geometry in Fig.A4. From this figure we have

$$\Delta x_o = s\Delta\alpha, \quad \text{and} \quad \Delta x = \Delta x_o \cos(\beta) \tag{A4a}$$

hence

$$\Delta x = s\cos(\beta)\,\Delta\alpha = h\,\Delta\alpha \tag{A4b}$$

therefore

$$\Delta x_1 = h\alpha_{8x}, \qquad \Delta x_2 = h\alpha_{7x} \tag{A5}$$

and h=607.44 inch.

Introducing (A5) to (A3) we obtain

$$\delta_z = \frac{h(\alpha_{7x} - \alpha_{8x})}{l} \tag{A6}$$

or, since $h/l = 1.245$, we found that

$$\delta_z = 1.245(\alpha_{7x} - \alpha_{8x}) \tag{A7}$$

Combining equations (A1), (A3), (A4) and (A7), the cross-elevation pointing error and the azimuth error are determined from the x-tilts of the inclinometers 1,2,7,8 as follows

$$\Delta_{xel} = 1.245(\alpha_{7x} - \alpha_{8x})\cos(\theta_{el}) - 0.5(\alpha_{1x} + \alpha_{2x})\sin(\theta_{el}) \tag{A8}$$

Appendix B.

Derivation of the Azimuth Axis Tilt from the Inclinometer Data

The inclinometer tilts caused by the azimuth axis tilt are described as

$$\alpha_{1x}(i) = a\cos(e(i) + \varphi), \quad \text{and} \quad \alpha_{1y}(i) = a\sin(e(i) + \varphi) \tag{B1}$$

or

$$\alpha_{1x}(i) = a_c c_i - a_s s_i, \quad \text{and} \quad \alpha_{1y}(i) = a_c s_i - a_s c_i \tag{B2}$$

where $a_c = a\cos(\varphi)$, $a_s = a\sin(\varphi)$, $c_i = \cos(e(i))$, and $s_i = \sin(e(i))$. For n samples we define the following vectors and matrices

$$\alpha_1 = \begin{Bmatrix} \alpha_{1x} \\ \alpha_{1y} \end{Bmatrix}, \quad \text{where} \quad \alpha_{1x} = \begin{Bmatrix} \alpha_{1x}(1) \\ \alpha_{1x}(2) \\ \vdots \\ \alpha_{1x}(n) \end{Bmatrix}, \quad \text{and} \quad \alpha_{1y} = \begin{Bmatrix} \alpha_{1y}(1) \\ \alpha_{1y}(2) \\ \vdots \\ \alpha_{1y}(n) \end{Bmatrix} \tag{B3a}$$

$$P = \begin{bmatrix} c & -s \\ s & c \end{bmatrix}, \quad \text{where} \quad c = \begin{Bmatrix} c_1 \\ c_2 \\ \vdots \\ c_n \end{Bmatrix}, \quad \text{and} \quad s = \begin{Bmatrix} s_1 \\ s_2 \\ \vdots \\ s_n \end{Bmatrix} \tag{B3b}$$

and

$$A = \begin{Bmatrix} a_c \\ a_s \end{Bmatrix} \tag{B3c}$$

For the above notations Eqs.(B2) can be re-written in a compact form

$$PA = \alpha_1 \tag{B4}$$

The least-square solution A of Eq.(B4) is as follows

$$A = (P^T P)^{-1} P^T \alpha_1 \tag{B5}$$

But, from Eq.(B3c) it follows that

$$a\cos(\varphi) = A_{11}, \quad \text{and} \quad a\sin(\varphi) = A_{21} \tag{B6}$$

therefore

$$a = \sqrt{A_{11}^2 + A_{21}^2}, \quad \text{and} \quad \varphi = \tan^{-1}\left(\frac{A_{21}}{A_{11}}\right) \tag{B7}$$

FIGURE CAPTIONS:

Figure 1. The 34-meter Deep Space Network antenna.

Figure 2. Inclinometer locations on the alidade structure.

Figure 3. Repeatability of the inclinometers readings, inclinometer No.1, *x*-tilt.

Figure 6. *y*-tilt of the inclinometer No.1 due to the thermal deformations of the alidade.

Figure 5. Tilts of the inclinometer No.2, and the azimuth correction angle

Figure 6. *x*-, *y*-, and *z*-rotations of the alidade, and the cross-elevation correction angle.

Figure 7. Relationship between azimuth and cross-elevation errors

Figure 8. Alidade rotations: left side (top figure) and right side (bottom figure).

Figure 9. Rotations of the middle bar of the alidade, and the average rotation of the alidade: left side (top figure) and right side (bottom figure)..

Figure 10. *x*-, *y*-, and *z*-rotations of the top of alidade due to azimuth track unevenness.

Figure 11. Azimuth track unevenness profile.

Figure 12. Inclinometer No1 tilt and the azimuth axis tilt (a), and the inclinometer No1 tilt with the azimuth axis tilt removed (b).

Figure 13. Inclinometer No2 tilt and the azimuth axis tilt (a), and the inclinometer No2 tilt with the azimuth axis tilt removed (b).

Figure 14. Pointing errors obtained from the azimuth correction table (solid line), and from the conscan measurements (dots): cross-elevation error for azimuth angle 300-340 deg (a), cross-elevation error for azimuth angle 0-60 deg (b), elevation error for azimuth angle 300-340 deg (c) and elevation error for azimuth angle 0-50 deg (d).

Figure A1. Determination of the *z*-rotation of the top of alidade.

Figure A2. Rigid-body rotation of the alidade side.

Figure A3. Deformation of the alidade due to a single wheel vertical displacement.

Figure A4. Determination of the alidade rotation.

FIGURE 1

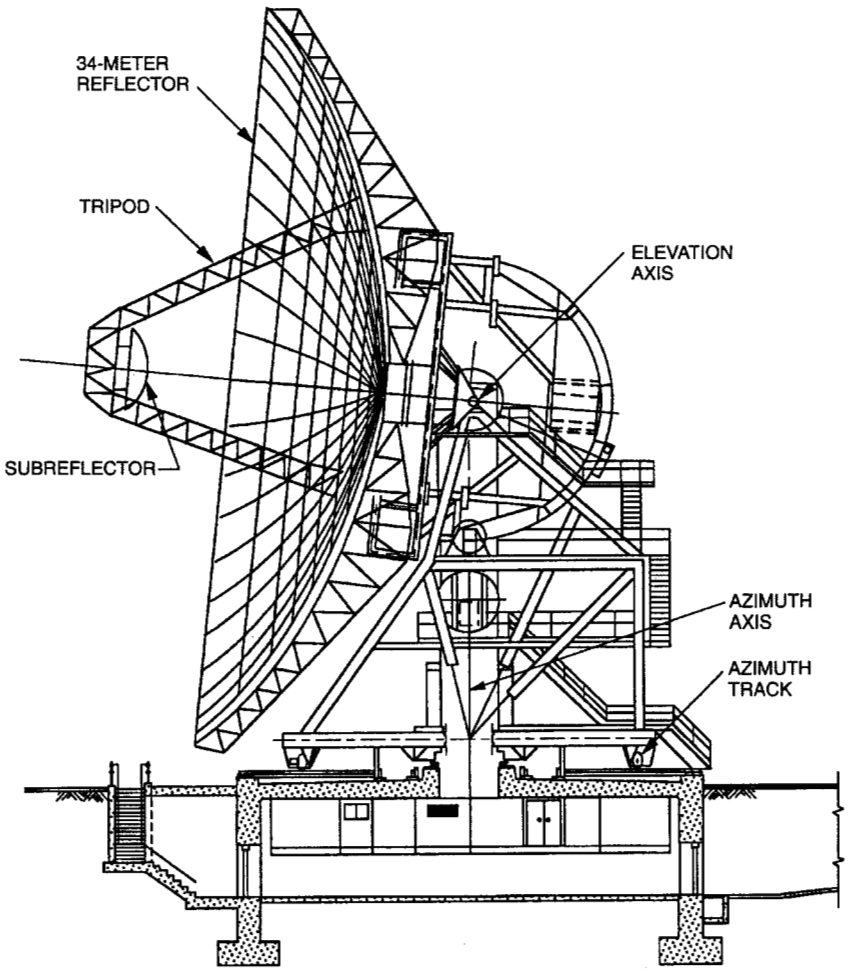
34-METER
REFLECTOR
TRIPOD
ELEVATION
AXIS
SUBREFLECTOR
AZIMUTH
AXIS
AZIMUTH
TRACK

FIGURE 2

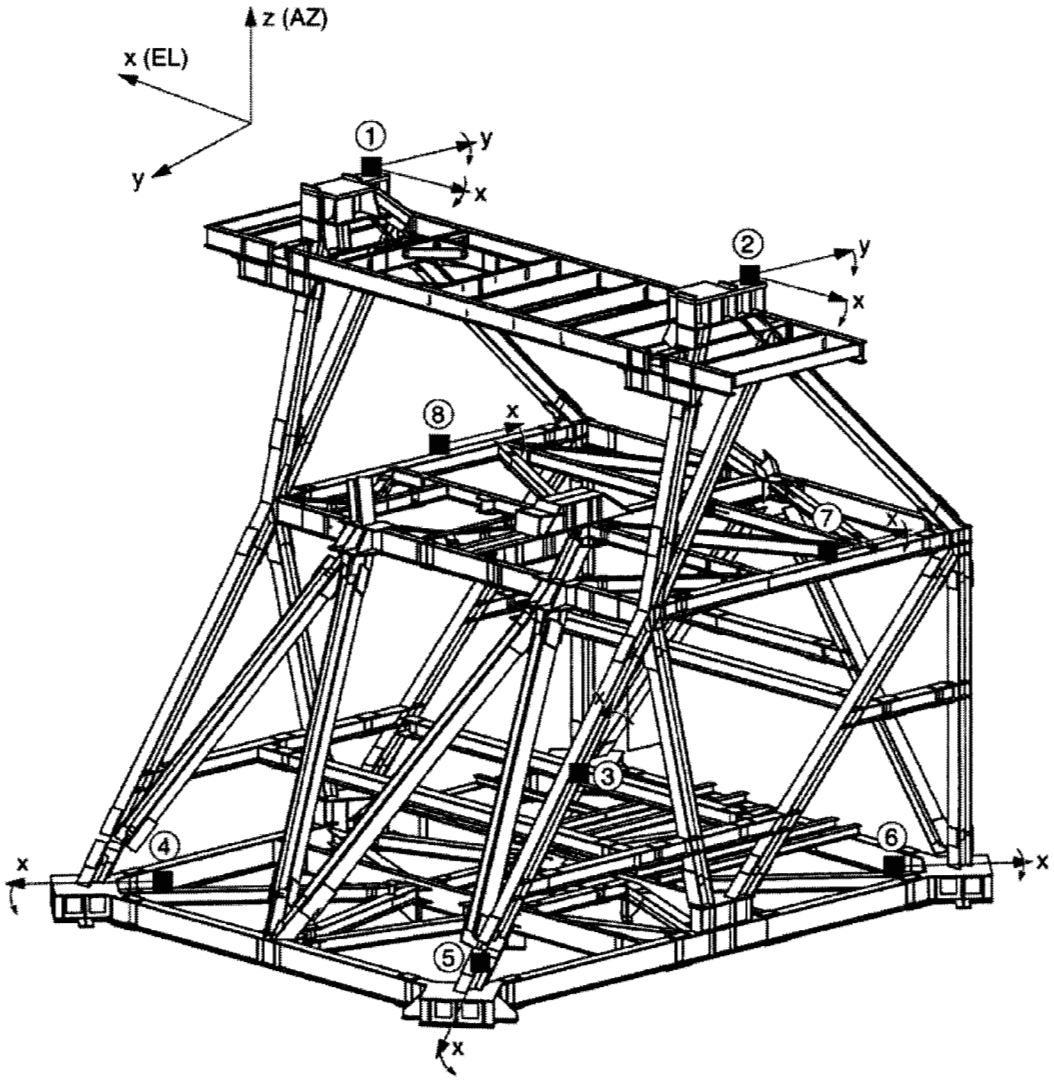

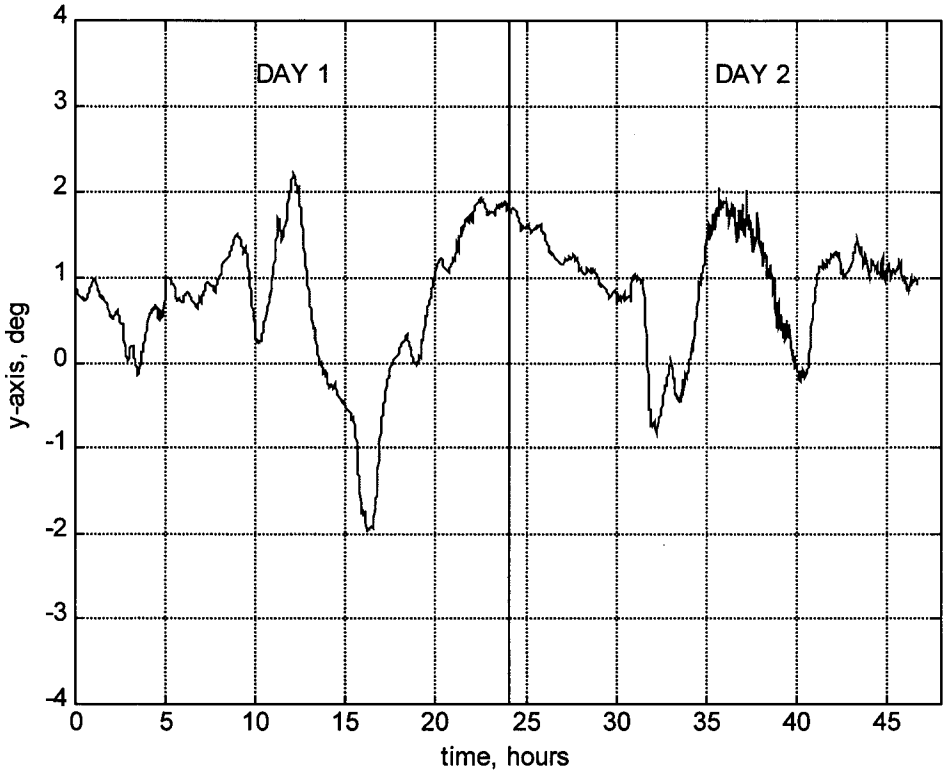
DAY 1
DAY 2
y-axis, deg
time, hours
4
3
2
1
0
-1
-2
-3
-4
0
5
10
15
20
25
30
35
40
45

FIGURE 4

FIGURE 5

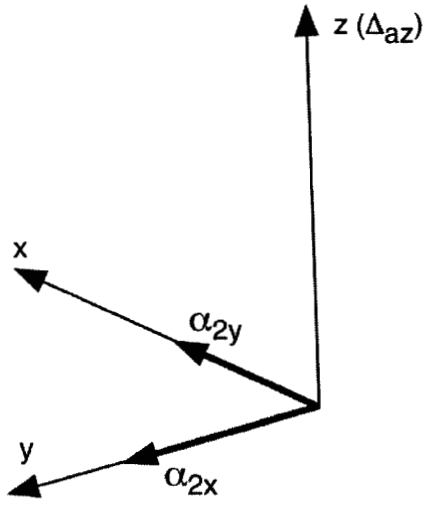

FIGURE 6

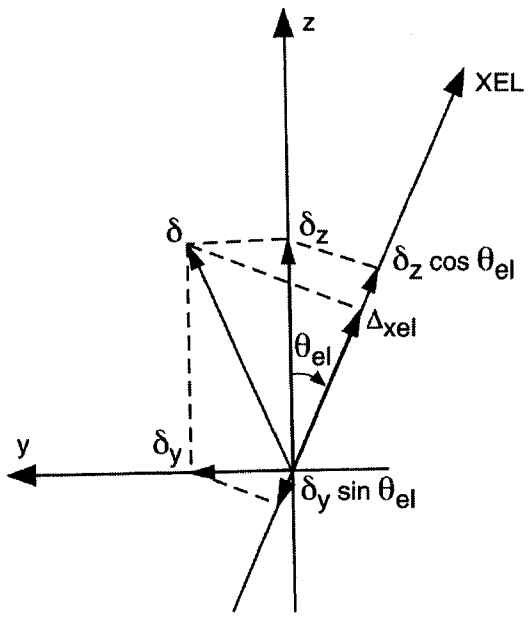

FIGURE 7

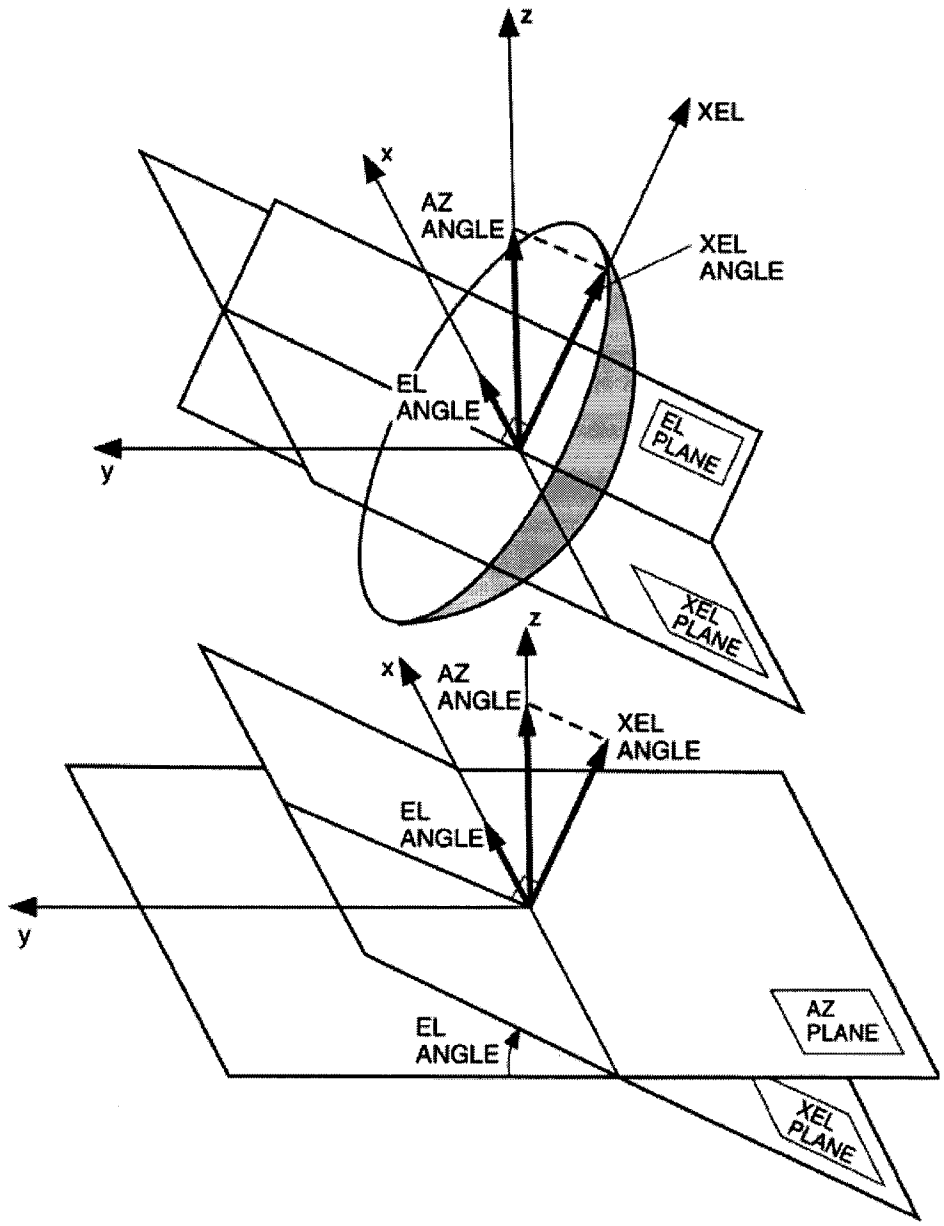
z
XEL
x
AZ
ANGLE
XEL
ANGLE
EL
ANGLE
EL
PLANE
y
XEL
PLANE
z
x
AZ
ANGLE
XEL
ANGLE
EL
ANGLE
y
AZ
PLANE
EL
ANGLE
XEL
PLANE

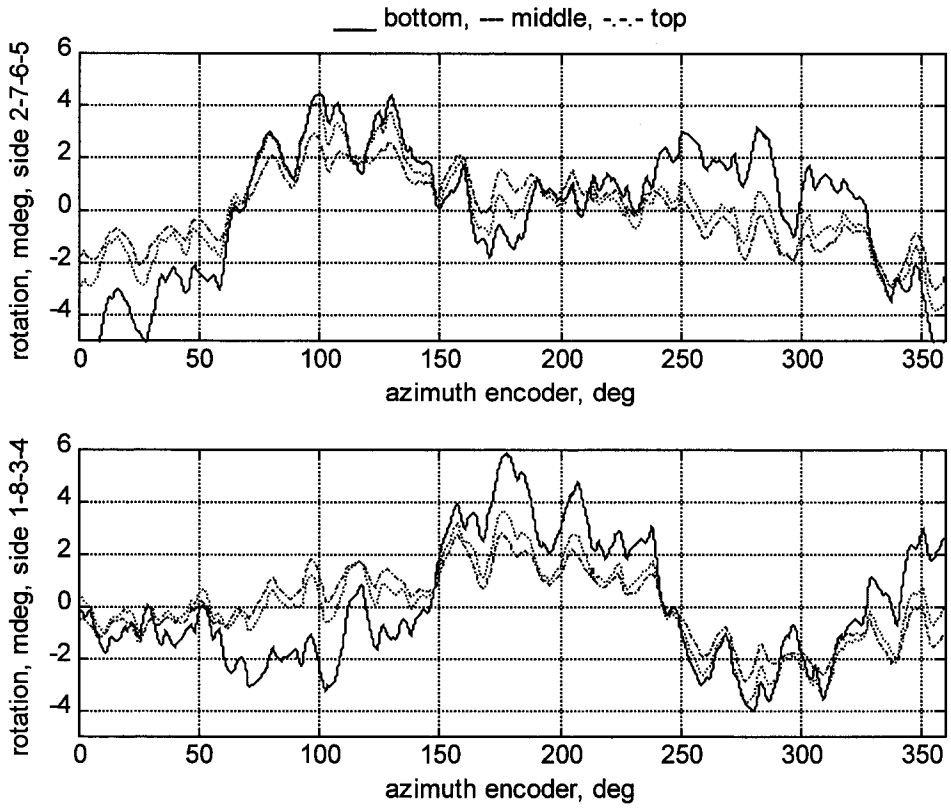
___ bottom, — middle, -.-.- top
rotation, mdeg, side 2-7-6-5
azimuth encoder, deg
rotation, mdeg, side 1-8-3-4
azimuth encoder, deg

FIGURE 8

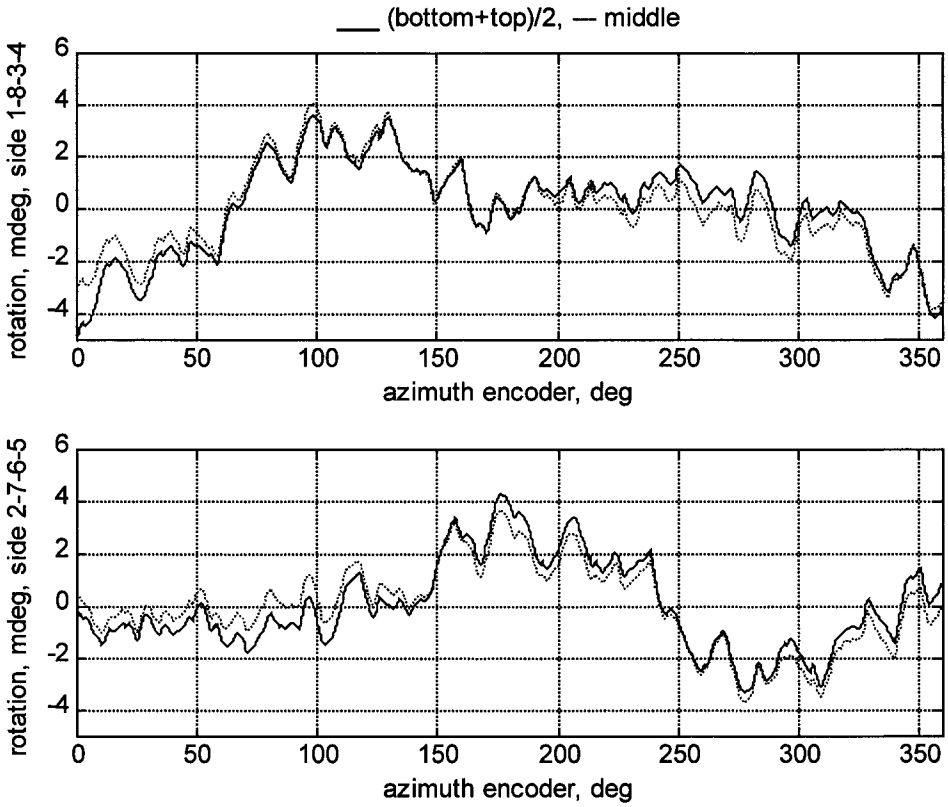
___ (bottom+top)/2, — middle
rotation, mdeg, side 1-8-3-4
azimuth encoder, deg
rotation, mdeg, side 2-7-6-5
azimuth encoder, deg

FIGURE 9

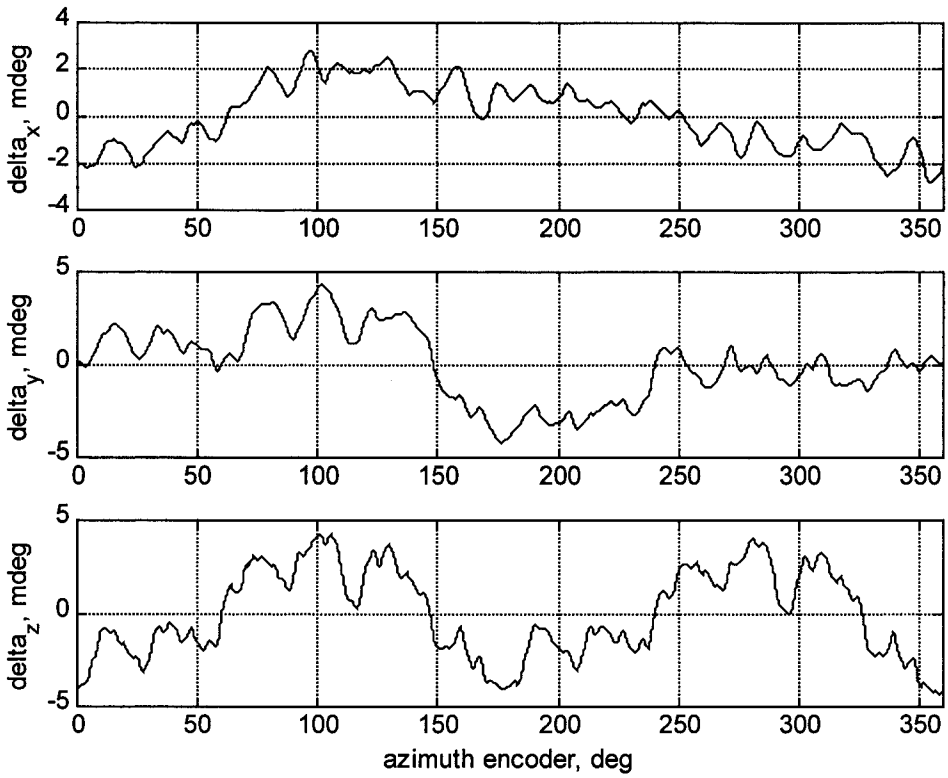

FIGURE 10

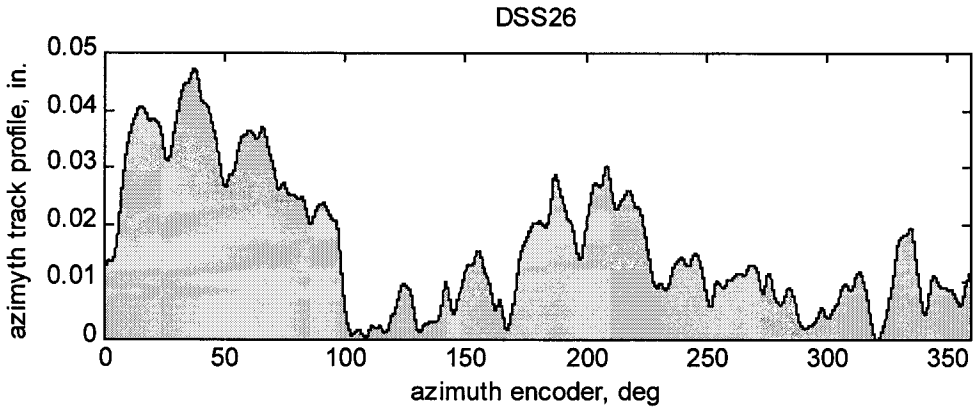
DSS26
azimyth track profile, in.
0.05
0.04
0.03
0.02
0.01
0
0
50
100
150
200
250
300
350
azimuth encoder, deg

FIGURE 11

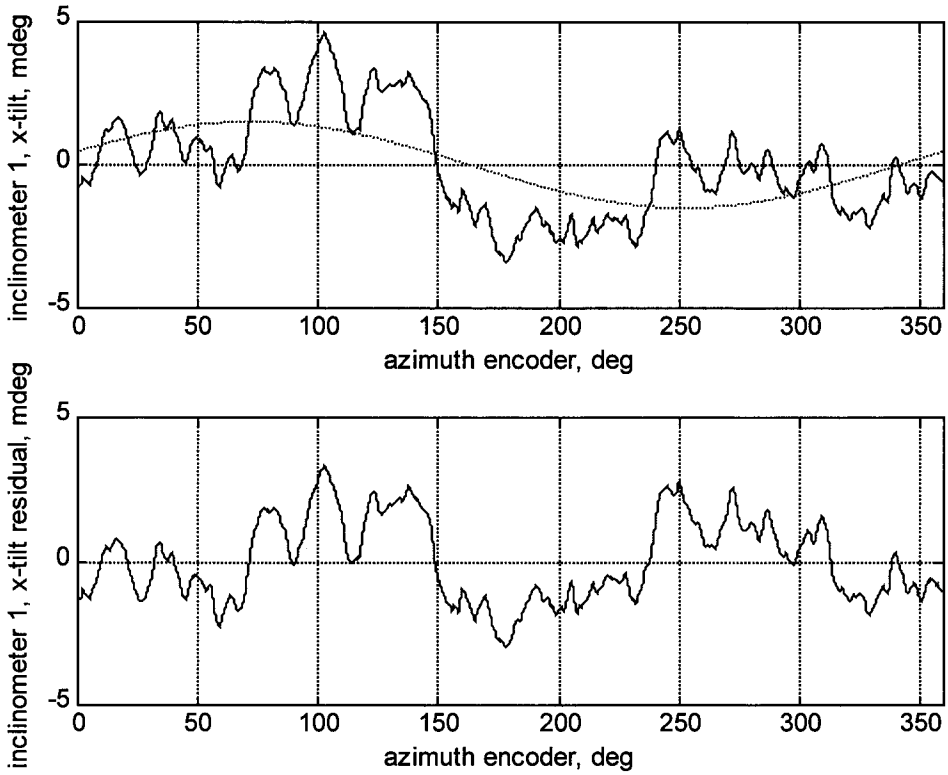
inclinometer 1, x-tilt, mdeg
5
0
-5
0
50
100
150
200
250
300
350
azimuth encoder, deg
inclinometer 1, x-tilt residual, mdeg
5
0
-5
0
50
100
150
200
250
300
350
azimuth encoder, deg

FIGURE 12

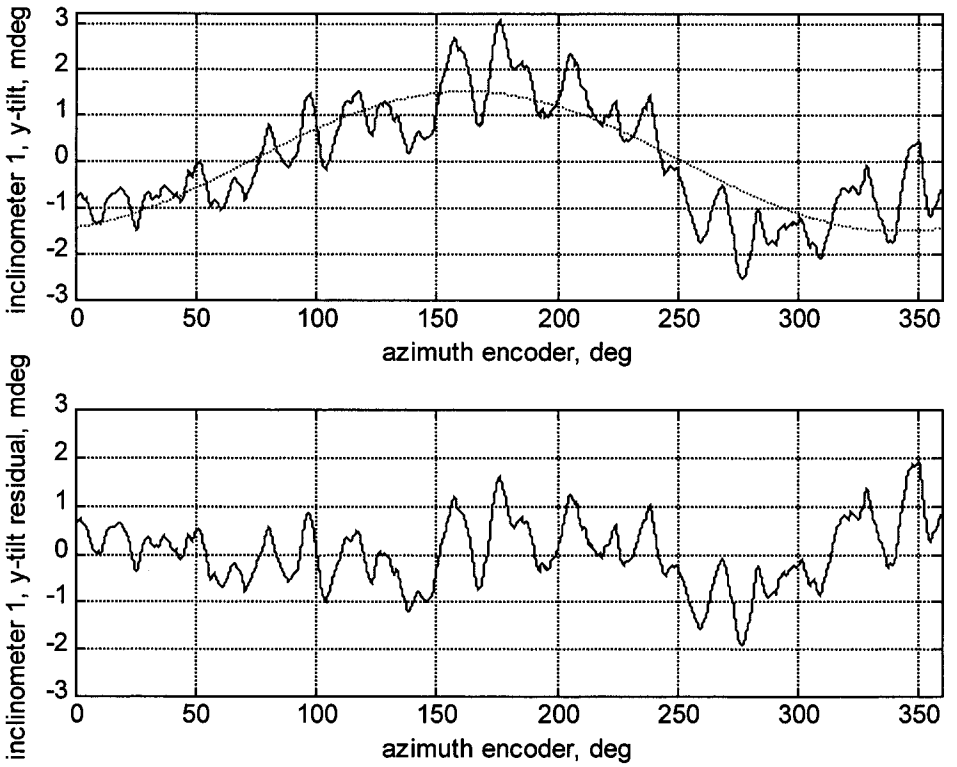
inclinometer 1, y-tilt, mdeg
3
2
1
0
-1
-2
-3
0
50
100
150
200
250
300
350
azimuth encoder, deg
inclinometer 1, y-tilt residual, mdeg
3
2
1
0
-1
-2
-3
0
50
100
150
200
250
300
350
azimuth encoder, deg

FIGURE 13

FIGURE 14

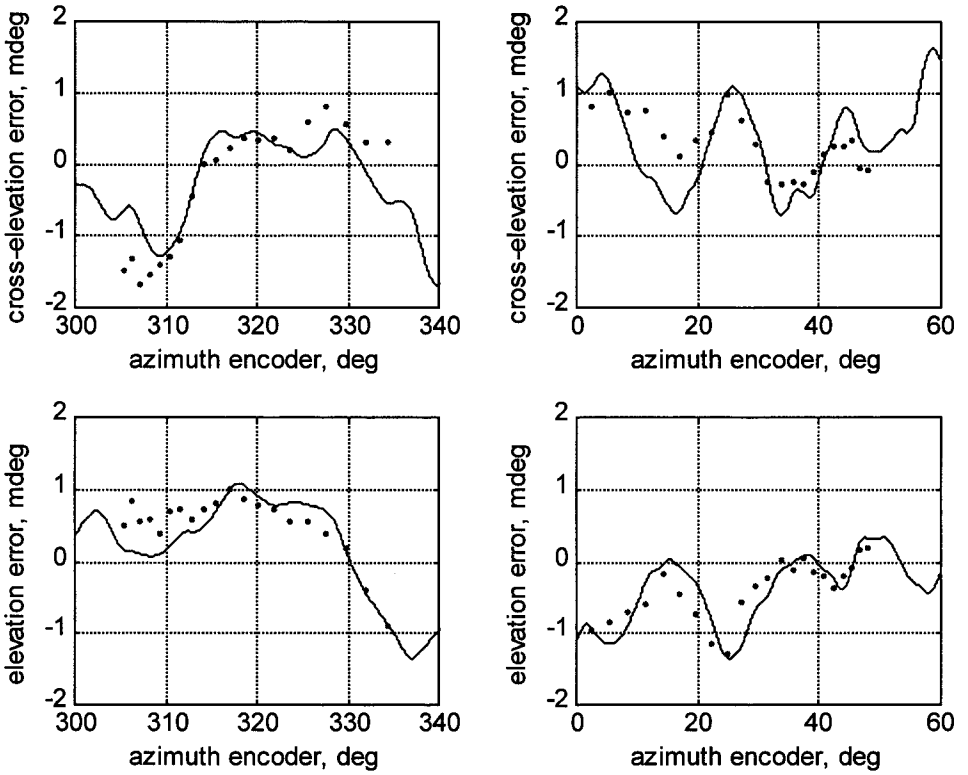
cross-elevation error, mdeg
2
1
0
-1
-2
300
310
320
330
340
azimuth encoder, deg
cross-elevation error, mdeg
2
1
0
-1
-2
0
20
40
60
azimuth encoder, deg
elevation error, mdeg
2
1
0
-1
-2
300
310
320
330
340
azimuth encoder, deg
elevation error, mdeg
2
1
0
-1
-2
0
20
40
60
azimuth encoder, deg

FIGURE A1

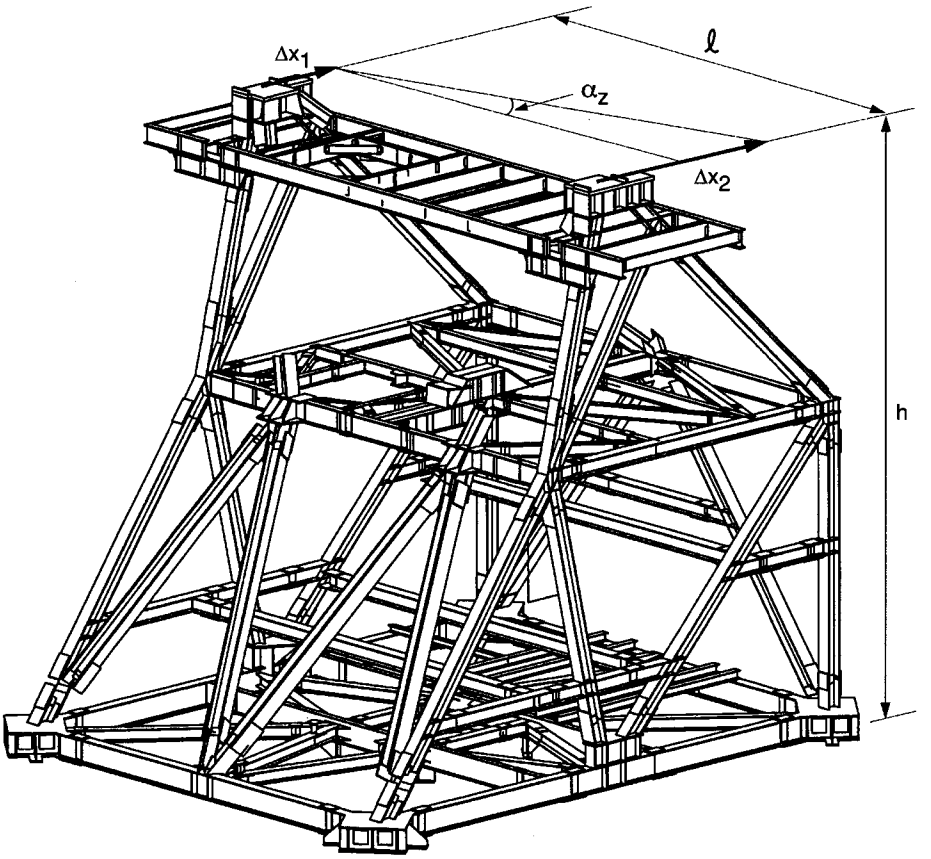

FIGURE A2

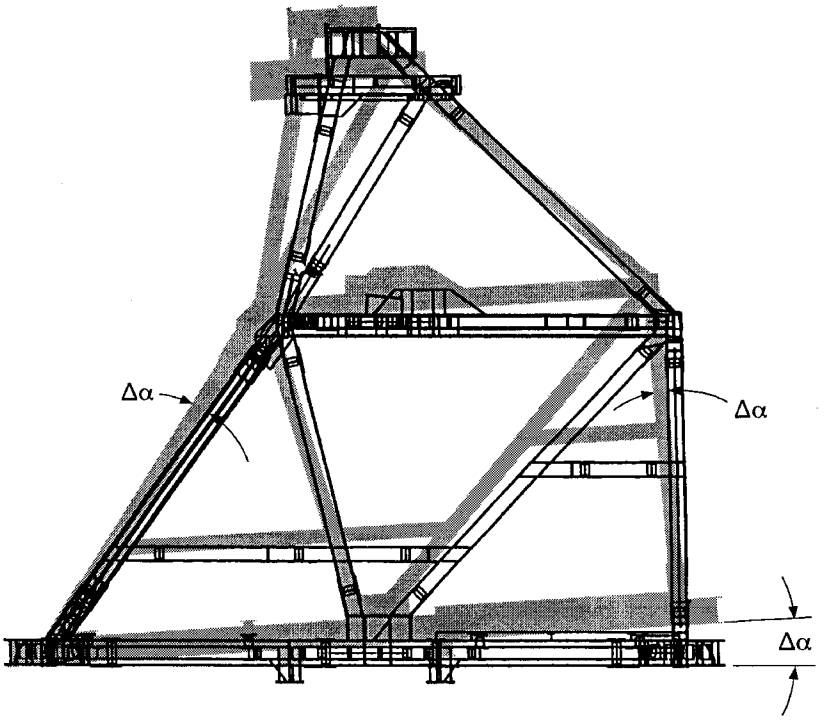

FIGURE A3

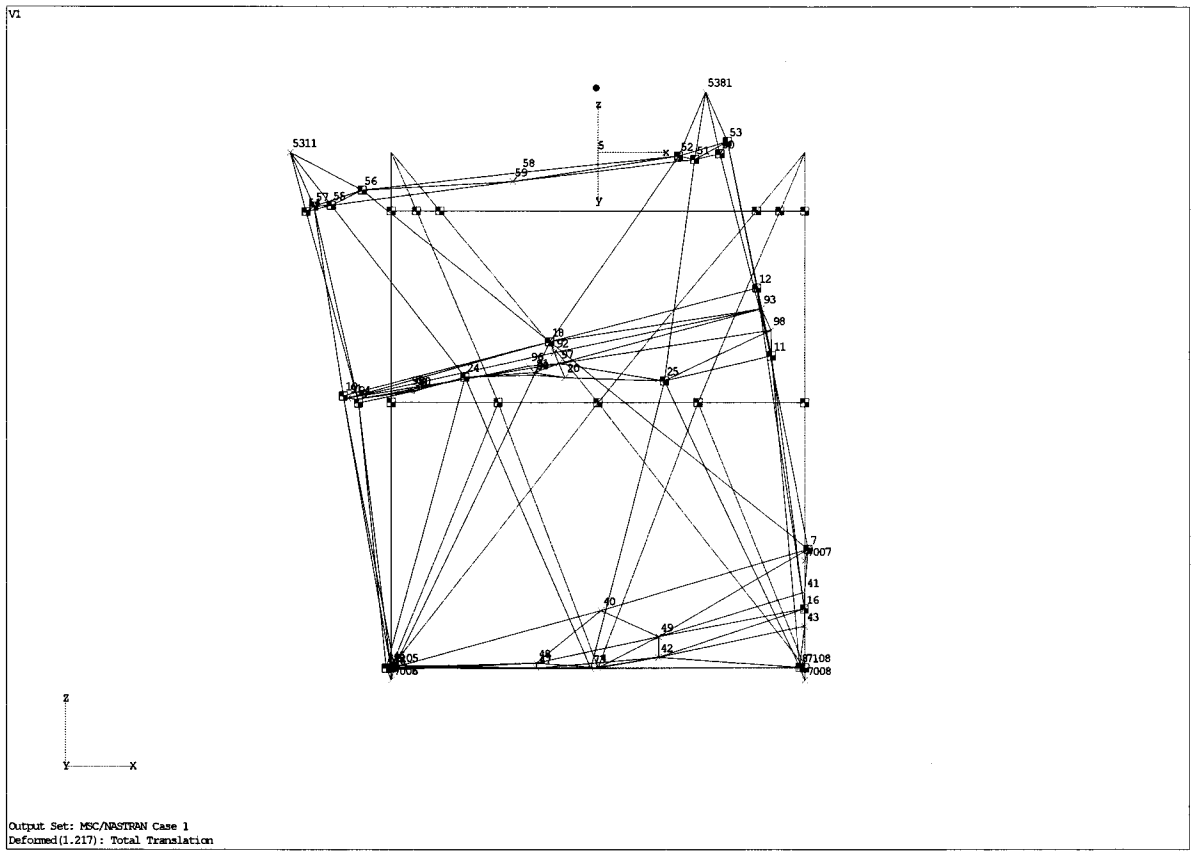
V1
5381
5311
53
58
59
56
57
55
12
93
98
11
28
92
97
20
25
24
7
41
16
43
40
49
42
Z
Y
X
Output Set: MSC/NASTRAN Case 1
Deformed(1.217): Total Translation

FIGURE A4

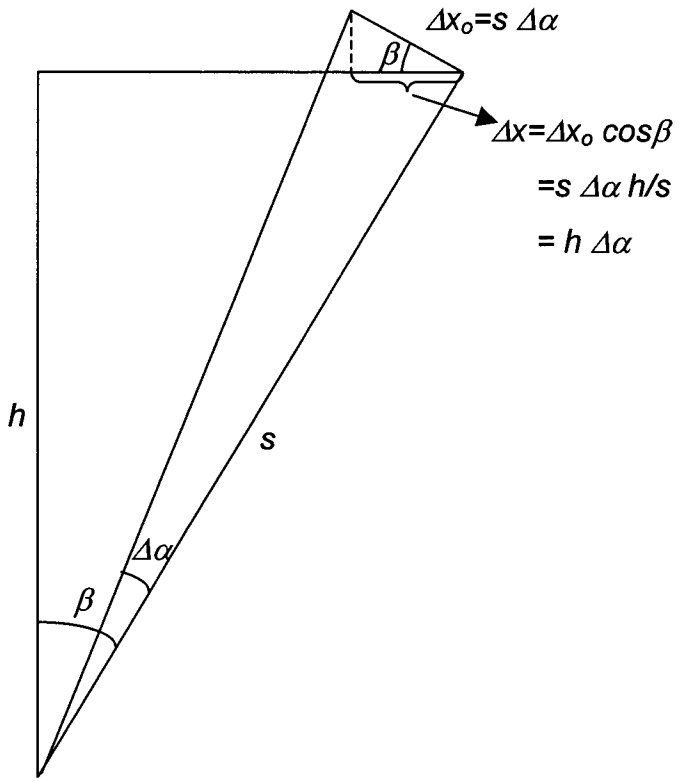
$\Delta x_o = s\,\Delta\alpha$
β
$\Delta x = \Delta x_o \cos\beta$
$= s\,\Delta\alpha\, h/s$
$= h\,\Delta\alpha$
h
s
$\Delta\alpha$
β